JOURNAL OF PROPULSION AND POWER
Vol. 14, No. 6, November–December 1998

Electrode Configuration Effect on the Performance of a Two-Dimensional Magnetoplasmadynamic Arcjet

I. Funaki,* K. Toki,† and K. Kuriki‡
Institute of Space and Astronautical Science, Kanagawa 229-8510, Japan

Thrust performance and internal plasma flowfield of a 1-MW class self-field magnetoplasmadynamic (MPD) arcjet were measured to evaluate their dependence on the cross-sectional geometry of the electrodes. A multichannel two-dimensional MPD arcjet in quasisteady operation was used to visualize the two-dimensional flowfield and reveal the correlation between the internal flowfield and the thrust performance. The experimental results for six different electrode configurations show that the thrust performance strongly depends on the thruster chamber cross-sectional geometries for the I_{sp} range of interest, 1000–3000 s. The cathode length determined the engine performance, regardless of the anode geometry. In particular, the convergent–divergent anode with a short cathode showed the best performance. The superior acceleration mechanism of the short cathode was explained on the basis of two-dimensional plasma distributions such as discharge current contours and plasma density obtained by Mach–Zehnder interferometry. A dense plasma region near the tip of the short cathode was observed and subsequent expansion guided by the diverging nozzle can enhance aerodynamic acceleration, which contributes to large thrust generation.

Nomenclature

c = speed of light, 3.00×10^8 m/s
d_a = effective anode separation, m
d_c = cathode diameter, m
e = elementary charge, 1.6×10^{-19} C
F = thrust, N
F_{em} = electromagnetic thrust, N
g = acceleration of gravity, 9.81 m/s^2
I_{sp} = specific impulse, s
J = total discharge current, A
L = plasma width, m
$\dot{m}$ = mass flow rate, g/s
m_e = electron mass, 9.11×10^{-31} kg
n_e = electron number density, m^{-3}
r_a = anode radius, m
r_c = cathode radius, m
TP = thrust to power ratio, mN/kW
V = discharge voltage, V
W = chamber width, m
x = electrode gap, m
α = nondimensional parameter in Eqs. (2) and (3)
$\Delta\phi$ = phase shift, rad
ε_0 = permittivity in vacuum, 8.85×10^{-12} F/m
η = thrust efficiency
μ = permeability in vacuum, 1.26×10^{-6} H/m
ν = light frequency of laser, Hz
ω_{pe} = electron plasma frequency, rad/s

Introduction

ELECTRIC rocket propulsion (EP) provides much higher specific impulse (I_{sp}) than chemical propulsion. One candidate electric propulsion system[1] is a self-field magnetoplasmadynamic (MPD) arcjet, which features a very wide I_{sp} range from 1000 to 7000 s, that can be easily covered by selecting propellant species and discharge current level. Steady-state MPD arcjets require extremely high-power levels because their thrust generation is based on the electromagnetic acceleration of the plasma created by high-current arc discharges and their self-induced magnetic field. To take advantage of the MPD thruster system within limited available power, pulsed operation using a capacitor bank is used. Such systems have been flight tested on several spacecraft including the electric propulsion experiment (EPEX) onboard the Space Flyer Unit, in which a pulsed 1-kW MPD thruster system was successfully tested in 1996.[2] Different from other EP systems, extrapolation of a low-power pulsed MPD technology to a higher power is easily accomplished by increasing the pulse frequency without any changes in its high-peak power, thruster performance, or size.[3] The relative simplicity, robustness, high-thrust density, high-power capability, ease of mission scaling, and reduced test facility requirements of pulsed MPD thrusters compared with other electric propulsion devices make them attractive for primary propulsion.

Specific missions of interest for MPD arcjets are manned or unmanned lunar and Mars missions, for which a multimegawatt steady-state MPD system with an I_{sp} of above 5000 s has been designed.[4,5] However, potential near-term application will be focused on the moderate I_{sp} regime of 1000–3000 s needed for orbital transfer missions. As far as a low-power spacecraft of several kilowatts is concerned, dc arcjets, ion thrusters, or Hall accelerators will be appropriate.[6,7] By contrast, when high power is available for a short mission time and large payload, advantages arise for the MPD arcjet.[8] As for the power regime of MPD operation, studies in the early 1980s indicated that the mass of the energy storage system was such that pulsed MPDs were ineffective against other EP systems at the power levels much below 100 kW.[9] Updated analysis for solar–electric orbit transfer, however, showed the competitiveness of even 10-kW-class low-power pulsed MPD system against dc arcjets in this moderate I_{sp} range and the power level.[10,11] Finding the best operational condition of the MPD arcjet will enhance the competitiveness toward other EP thrusters for this moderate I_{sp} and the power range beyond 10 kW.

To maximize the thrust efficiency, the best combination of propellant supply system, propellant species, and chamber geometry must be selected. This paper concentrates on the last

Received Feb. 2, 1997; revision received Feb. 24, 1998; accepted for publication June 15, 1998.

*Researcher, Space Propulsion Division, 3-1-1 Yoshinodai, Sagamihara. Member AIAA.
†Associate Professor, Space Propulsion Division, 3-1-1 Yoshinodai, Sagamihara. Member AIAA.
‡Professor, Space Propulsion Division. Fellow AIAA.

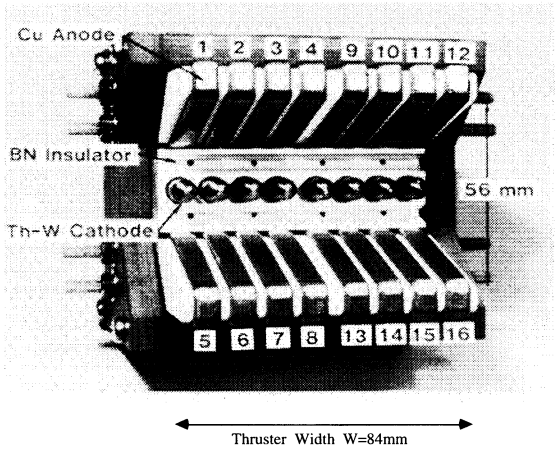

Fig. 1 Multichannel two-dimensional MPD arcjet.

two effects for a quasisteady self-field MPD arcjet. A comparison of NH_3, N_2H_4, Ar, N_2, and H_2 propellants showed that hydrogen and molecular gases containing hydrogen were superior to Ar.[12] In spite of large energy deposition into dissociation, electrothermally accelerated hydrogen yielded higher thrust than Ar did for the same mass flow rate and discharge current.[13] On the other hand, the design of the discharge chamber is rather ambiguous and most researchers have used converging–diverging[14] (Laval), flared,[15] and benchmark[15] configurations without deliberation. While the Laval nozzle anode geometry is still used, some reports concluded that the flared configuration with a short cathode showed better performance.[16] Uematsu et al.[16] and Yoshikawa et al.[17] showed that the thruster performance can be significantly improved via shortening the cathode, for H_2 and NH_3. However, with the short cathode configuration, it is possible that the high-density and high-temperature region appearing on the cathode tip produces compression shocks and, thereby, degrades aerodynamic acceleration.

In this paper, the effect of the discharge chamber geometry on the performance and the flowfield was studied for a self-field multichannel two-dimensional MPD arcjet (2D–MPD) shown in Fig. 1. This model is used only for research purposes and is not intended for flight application. Its low efficiency is caused by imperfect magnetic field containment compared with coaxial configurations. With the 2D–MPD, it is very difficult to reflect the features of coaxial devices; however, the easy access to the flowfield including laser diagnostics makes it possible to relate the flow data with the performance data. For Ar and H_2 propellants, thrust performance, current distribution, and plasma density distribution were obtained and compared for six chamber configurations. The correlation between the flowfield and thruster performance will be helpful, not only for making and/or checking a physical model inside the discharge chamber, but also for establishing a design approach for MPD arcjets.

Experimental Apparatus and Procedure

Two-Dimensional MPD Arcjet

The 2D–MPD arcjet provides a nearly two-dimensional flowfield with eight discharge channels, each of which has a centered 2% Th–W cathode and two Cu anodes.[18] Among geometric parameters, the cathode diameter and the anode opening at the inlet were 8 and 14 mm, respectively, as shown in Fig. 2, where the six cross-sectional types of the geometry for the discharge chamber are depicted. The thruster head was set in a stainless-steel vacuum tank of 0.8-m diam and 2.0-m length, which was evacuated to less than 7 mPa before each firing. The pressure reached 65 mPa immediately after firing.

A fast-acting valve (FAV) allowed us to provide gaseous propellants in rectangular waveform. The FAV simultaneously

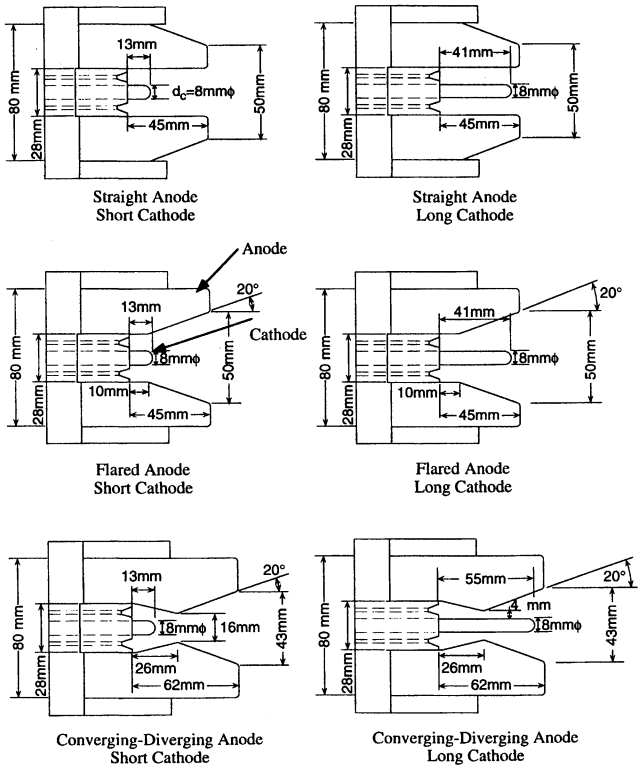

Fig. 2 Cross-sectional geometry of electrodes.

opens and closes eight valves, and the gas in the reservoir flows through choked orifices of 0.6 mm in diameter. A gas pulse of about 5-ms duration was then introduced into the chamber by eight gas ports located between the anodes and cathodes. After the gas pulse reaches its quasisteady state, the ignitron of a pulse-forming network (PFN) is triggered. The PFN supplies the discharge current with a 0.5 ms flat-topped waveform of 7–19 kA in the quasisteady mode. Once the PFN is triggered, arc breakdown is automatically introduced by more than 2-kV charging voltage. Channel-to-channel discharge uniformity was achieved by forcing the total discharge current through 16 equally divided 1.25 Ω resistors. Its uniformity was confirmed by showing that the voltage waveform for all channels was the same; the channel-to-channel variation of voltage was less than 5%.[18]

Ar and H_2 were specified as the propellant gases. The mass flow rates were controlled by adjusting the reservoir pressures, and their steady-state values were chosen as $\dot{m}$ = 0.625, 1.25, and 2.5 g/s.

Measurement Methods

Thrust measurements are carried out by the parallelogram–pendulum method. The 2D–MPD arcjet and the FAV were mounted on a thrust stand suspended with four steel wires. The impulse was found from the maximum amplitude of its swing; after subtracting cold impulse bit, it was transformed into thrust by dividing the quasisteady duration. The displacement of the pendulum was measured with a laser position sensor. For the calibration of the pendulum and position sensor combination, impulses of known magnitude were applied to the target of the thruster. A simple pendulum consisting of a steel ball and a string was used in an atmospheric pressure environment, and the impulses of the ball were calculated from its mass and striking velocity evaluated from the energy conservation for the calibration pendulum. Because of uncertainty of the estimated velocity, the impulse measurement was accurate to within ±1%. The discharge current was measured by a Rogowski coil with an integrating circuit calibrated with a known shunt resistance. Voltage measurement was performed with a voltage probe, which detects the small current bled through a known resistor (10 kΩ) between the electrodes. The

output signals of both the discharge current and the discharge voltage were recorded on the digital memory at the acquiring speed of 1 word/μs. Because of rounded 8-bit data, the accuracy of voltage and current were $\pm 0.5\%$. Major errors in the thrust and the discharge voltage measurement come from shot-to-shot deviations, which were less than 5% of the averaged value of more than five shots. For the total current measurement, such shot-to-shot error was less than 1%.

Averaged values of the mass flow rate were confirmed from the rectangular pulse shape determined by the pressure gauge and the measured reduction of the reservoir pressure for several shots. Shot-to-shot uncertainty of the mass flow was below 5%, which was estimated from the impulse of the cold gas.

The method for the internal flow measurement was the same as that described in Ref. 19. Briefly, the 2D–MPD can be divided into two pieces by the vertical plane, and probes sandwiched between two 1-mm-thick quartz glasses can be inserted into the opening. For the current contour line measurement, magnetically sensitive film with microencapsulated iron needles was inserted. The magnetic field strength was detected by darkness patterns that could be calibrated by known strength of magnetic fields. The darkness pattern was analyzed by an image processor that can resolve up to 1.5×10^{-3} T, though nonuniformity in the light source of the image scanner increased the uncertainty to $\pm 6.0 \times 10^{-3}$ T.

The electron density distribution was measured by Mach–Zehnder interferometry. Considering that the ion plasma frequency is much lower than the electron plasma frequency and that effect of the electron thermal velocity and magnetic field in the wave propagation direction is negligible, the phase shift caused by the electron is written by

$$\Delta\phi = \omega_{pe}^2 L/4\pi\nu c \tag{1}$$

where the electron plasma frequency is

$$\omega_{pe} = \sqrt{n_e e^2/m_e \varepsilon_0}$$

The electron density can be directly evaluated from this equation because of a negligible contribution of the phase shifts from atoms or molecules. Because of the low plasma density of about 10^{21} m^{-3} with an optical length of 8.4 cm, CO_2 laser interferometry with a wavelength of 10.6 μm was required to obtain a 0.5 fringe shift. A Lumonics® CO_2 transversely excited atmospheric (TEA) laser beam was introduced through a germanium window to the vacuum chamber, in which a major optical frame was mounted on an aluminum plate. The fringe was displayed on a liquid crystal film, which is sensitive to infrared light, showing fringe patterns as colored reflection. The image of the fringe pattern was processed by an image scanner and a microcomputer to evaluate plasma density from the fringe shift. Two error sources were considered. One is the fringe shift by other particles except electrons, which amounts to a 10% density error for neutral molecules and atoms, and a 2% error for ions. The other is associated with the resolution of the data acquisition system. Because the maximum resolution of the density measurement was 0.1 fringe shift (2.3×10^{20} m^{-3}), Ar's fringe shift of below 0.3 (6.9×10^{20} m^{-3}) cannot be precisely captured. This resolution limit causes a 50% density error for Ar, and a 15% error for H_2.

Experimental Results and Discussion

The thrust performance data were evaluated in terms of η, I_{sp}, and TP, which are defined as follows:

$$\eta = F^2/2\dot{m}JV = \frac{g}{2} I_{sp} \cdot TP, \qquad I_{sp} = F/\dot{m}g, \qquad TP = F/JV$$

Comparison Between Argon and Hydrogen

In Fig. 3, all of the measured thrust efficiencies for all configurations are grouped into Ar and H_2, and are plotted against

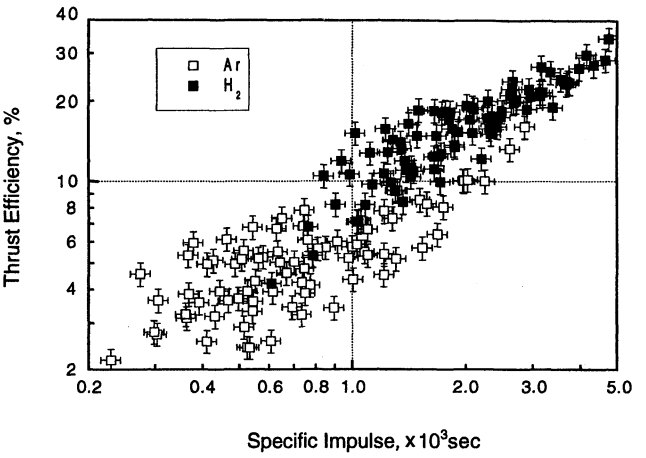

Fig. 3 Thrust efficiency vs I_{sp} plot for comparison between Ar and H_2.

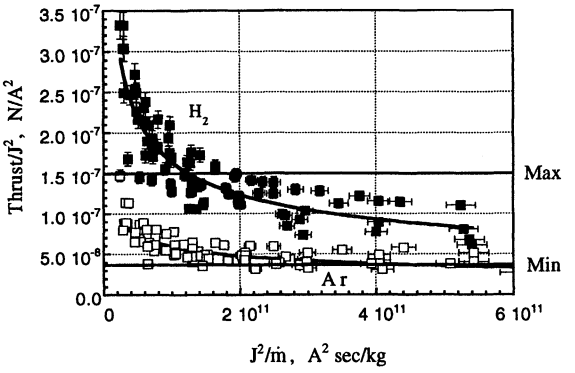

Fig. 4 Thrust scaling [Max, Min are theoretical predictions based on Eq. (2)].

I_{sp}. Here high efficiency means high-thrust efficiency or high-thrust-to-power ratio for a given specific impulse; the efficiencies for H_2 propellant surpassed that for Ar because of the large-thrust generation of H_2, as shown in Fig. 4, where the thrust for H_2 is nearly twice as large as that for Ar.

Theoretical Magnetic Thrust of 2D–MPD and Thrust Characteristics

Thrust characteristics for H_2 and Ar are summarized in Fig. 4, which shows the scaling law of thrust for both propellants. Solid lines in the figure, Max and Min, represent the electromagnetic thrust of 2D–MPD calculated as a function of J^2 (Ref. 20):

$$F_{em} = (\mu J^2/4W)[x + \alpha(d_c/2)] \tag{2}$$

where x is the electrode gap along an effective discharge current path for two limiting cases: $x = (d_a - d_c)/2$ for Min with $d_a = 28$ mm and $d_c = 8$ mm, and $x = d_a/2$ for Max with $d_a = 50$ mm for the straight anode and $d_a = 80$ mm for the flared or the converging–diverging anode. Min corresponds to the condition that the current path is confined to within the equal channel spacing, whereas Max applies to the case in which the discharge current extends outside the discharge chamber and attaches at the far downstream end of the anode.

The second term on the right-hand-side of Eq. (2) is attributed to the so-called pumping force, which depends on the ratio of inflow current into the cathode tip: $\alpha = 0$ means no current into the tip, whereas $\alpha = 1$ specifies that all current flows into the tip.

An important difference between the 2D–MPD and coaxial MPD arcjets is the stronger dependence of the 2D–MPD on

its chamber geometry. For coaxial-type MPD thrusters, the theoretical electromagnetic thrust is given by the equation[1]

$$F_{em} = (\mu/4\pi)J^2[\ln(r_a/r_c) + \alpha] \quad (3)$$

where thrust depends on the logarithm of the ratio of r_a to r_c, in contrast to the 2D–MPD, which generates thrust linearly proportional to an electrode separation.

Figure 4 illustrates the scaling of thrust for the 2D–MPDs tested. It is clear that 1) H_2 produces much more thrust than Ar over a wide range of $J^2/\dot{m}$; 2) this difference is especially large at smaller $J^2/\dot{m}$; 3) F/J^2 of each gas approaches a constant value at large $J^2/\dot{m}$, and the thrust tends to show J^2 dependence there; and 4) even at high $J^2/\dot{m}$ values, H_2 remains superior to Ar.

Because a J^2 thrust dependence such as those mentioned in item 3 characterizes the dominance of electromagnetic effects in thrust generation, any thrust above the theoretical electromagnetic force limit (Max) must be attributed to an aerodynamic contribution that originates from the thermal expansion of high-enthalpy plasma. Both propellants, particularly H_2, generate very large thrust at a low $J^2/\dot{m}$ parameter. This large electrothermal thrust component of H_2 leads to the large difference between the two propellants.

Referring to the items 3 and 4, a thrust generation of H_2 keeps its advantage even at the electromagnetic dominant operation. Figure 5 shows the difference of discharge patterns between H_2 and Ar, in particular, the large downstream current extension of H_2 is contrasting with the upstream current concentration with Ar. This downstream extension results in a large effective d_a and, hence, large x in Eq. (2), which corresponds to strong electromagnetic blowing thrust. At higher $J^2/\dot{m}$, H_2 still keeps its feature of high thrust, except for the case of the converging–diverging anode, and thereby retains the superiority by means of large electromagnetic thrust.

Comparison Between Short and Long Cathode

Differences were found between operation with the short cathodes and the long cathodes. Geometric dependence can be evaluated in Figs. 6–9. Figure 6 shows the thrust efficiency characteristics of H_2; at the medium-I_{sp} range between 1000 and 3000 s, the efficiencies of the short cathodes are obviously superior to those of the long cathodes, in particular, the converging–diverging anode and short cathode shows the best performance. At a higher I_{sp} beyond 3000 s, the thrust efficiency vs I_{sp} curves tend to show a constant thrust-to-power ratio and do not exhibit a strong dependence on the chamber geometry. These features agree qualitatively with experimental results for the coaxial-type thrusters presented in Ref. 16. In the case of Ar shown in Fig. 7, the short cathodes give superior performance over long ones for a given anode configuration. From the comparison of the short and long cathode configurations, one can conclude the superiority of the short cathodes regardless of the anode configuration, and the converging–diverging shows good performance at the medium I_{sp} range of 1000–3000 s.

The advantage of the short cathodes is attributed to their large-thrust generation and/or their low-discharge voltages as demonstrated in Fig. 8 (for $\dot{m} = 2.5$). The thrust characteristics of the short cathode are superior to those of the long cathode for both propellants, the only exception being the flared anode for H_2. This tendency is independent of anode geometry, and the thrust of a short cathode configuration is always larger than that of a long cathode, resulting in high-thrust efficiency. Furthermore, the discharge voltage of the short cathodes for H_2 is lower than that for the long cathodes, whereas the reverse is true for Ar. In Fig. 8b, the linear variation of voltage with

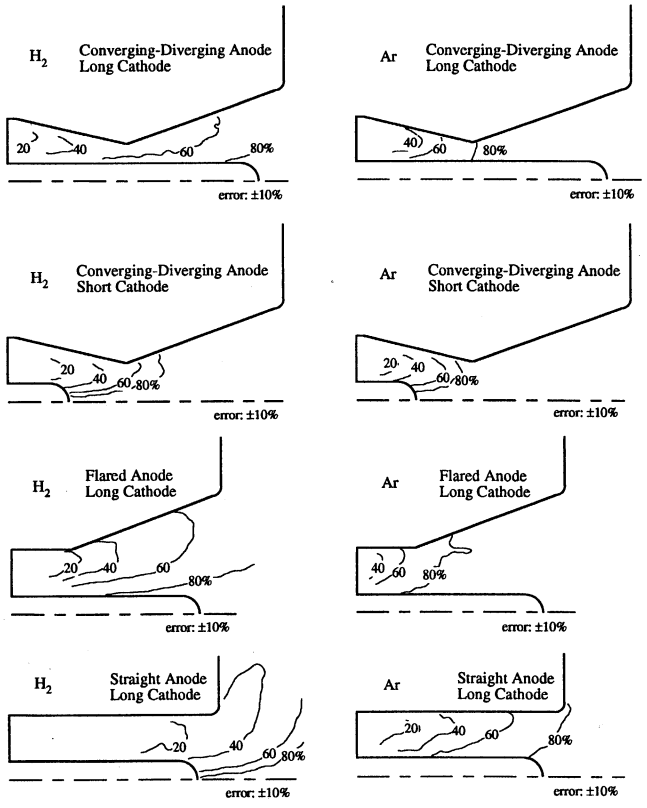

Fig. 5 Current distribution (J = 12 kA, $\dot{m}$ = 1.25 g/s).

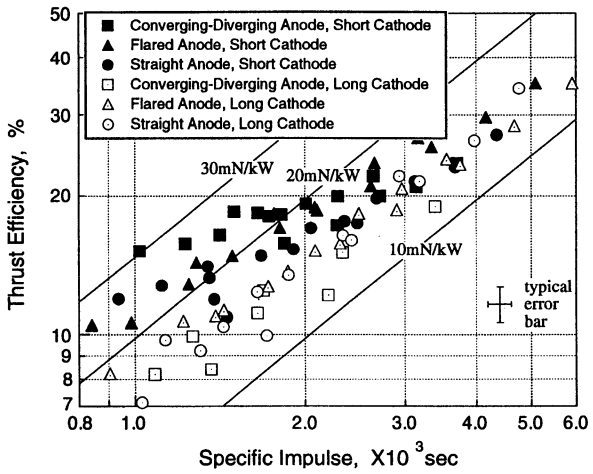

Fig. 6 Thrust efficiency vs I_{sp} plot for H_2, comparison of six geometries.

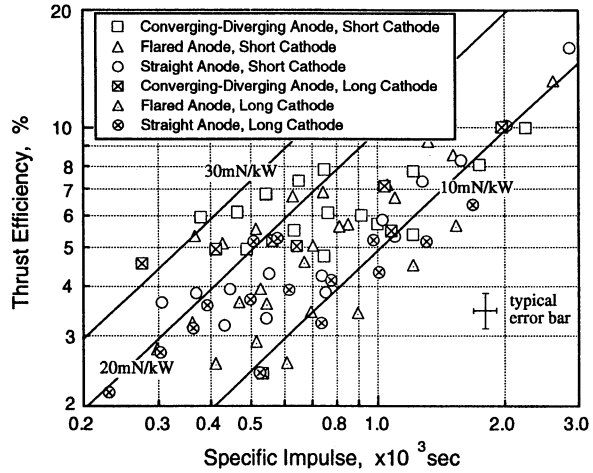

Fig. 7 Thrust efficiency vs I_{sp} plot for Ar, comparison of six geometries.

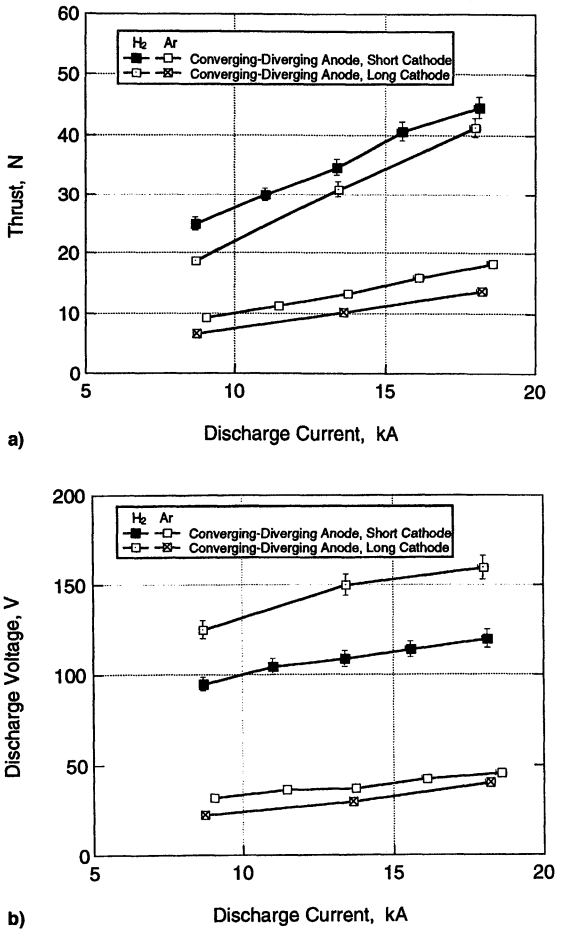

Fig. 8 Short and long cathode comparison of a) thrust and b) voltage ($\dot{m}$ = 2.5 g/s).

current suggests a large aerodynamic thrust contribution, which was also indicated earlier, based on the thrust characteristics.

The plasma density distributions of several configurations are compared in Fig. 9. The gas selection drastically changes the plasma density distribution; H_2 features its large density region near the cathode tip, whereas for Ar, the plasma density distribution shows a relatively high-density region only near the cathode corner followed by sudden expansion. These features were enhanced in the case of the converging–diverging anode with a short cathode; the dense plasma because of compression of the plasma and/or the current concentration was observed at the anode throat, after which the plasma was accelerated with the assistance of aerodynamic forces from the diverging nozzle. In this way, a large contribution of aerodynamic thrust is expected in the case of converging–diverging nozzle.

Flow Structure near the Cathode Tip

Aside from rating the geometry of the 2D–MPD, the plasma flowfield for the short cathode can be described as follows. For Ar, most of the ionization takes place near the inlet, and the plasma is easily accelerated to supersonic speeds there. This is a typical explanation for acceleration process in the analysis of MPD thruster flow.[21] After the supersonic expansion at the cathode shoulder, the plasma flows into the cathode tip at a supersonic speed. Consequently, a compression oblique shock, which will deteriorate the aerodynamic acceleration, may be induced emerging from the cathode tip for Ar. However, such a shock structure was not found in Fig. 9. No existence of a shock wave implies subsonic flow merging into the centerline, or even in the case of supersonic flow, only a very weak shock may be hidden within the resolution limit. It

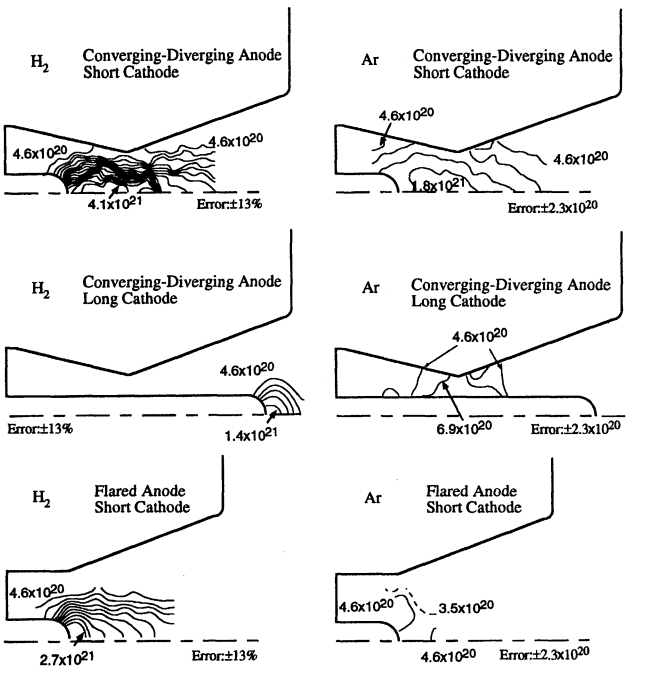

Fig. 9 Density distribution (J = 12 kA, $\dot{m}$ = 1.25 g/s, unit = m^{-3}).

is also possible that diffusive effects spread the thickness of the shock, or the complicated boundary effect around the multiple cathodes destroys a two-dimensional shock structure. It should be noted that, strictly speaking, that the word *sonic* must be considered as magnetogasdynamic and should be replaced by *magnetosonic*.

For H_2, the sonic passage will occur at the downstream discharge region. After being ionized near the cathode tip, and being free from a shock, the hydrogen plasma will smoothly accelerate, both electromagnetically and aerodynamically.

Design Guidelines for MPD Arcjet

It may be difficult to predict the geometric dependence of the performance and the flowfield of coaxial thrusters from the experimental data based on the 2D–MPD. Nevertheless, it is useful to think about possible improvements for more efficient thrusters by comparing the coaxial and the 2D–MPD thruster. Regarding the gas selection, hydrogen is strongly recommended because of 1) a large electromagnetic thrust compared with argon resulting from the enlarged effective discharge path and the strong pinch effect at the cathode tip associated with real gas effect,[22] and 2) its large aerodynamic thrust generation. However, the former mechanism is not so effective in coaxial MPDs because the logarithmic scaling effect of the electromagnetic thrust is a weak function of the anode-to-cathode-diameter ratio. As a result, the enhancement of the electromagnetic thrust is possible only with increasing the discharge current but not by means of geometric variation. Furthermore, dominance of electromagnetic thrust arose near the onset points, above which neither stable operation nor thrust generation proportional to J^2 is expected. Therefore, as far as medium operational I_{sp} less than 3000 s is concerned, one cannot rely on the dominance of the electromagnetic thrust, but should rely on the enhancement of electrothermal thrust for the improvement of the thrust generation of self-field MPD arcjets. The convergent–divergent anode with the short cathode is the appropriate geometry to enhance the aerodynamic acceleration through the anode throat as well as its self-field magnetic nozzle.

Summary and Conclusions

Thrust performance and flowfield measurements of self-field two-dimensional MPD arcjets were made and the dependence

of its thrust efficiency on the cross-sectional geometry of the discharge chamber was evaluated. The thrust efficiency was greatly influenced by the gas selection; between the two propellants, thrust obtained with hydrogen is twice as large as that of Ar because of its large magnetic and aerodynamic thrusts, which results in high efficiency. In the medium-I_{sp} range between 1000 and 3000 s, the short cathodes are superior to the long cathodes, whichever anode geometries are converging–diverging, flared, and straight. Beyond 3000 s, however, thrust efficiency vs I_{sp} curves were only slightly affected. The converging–diverging anode with a short cathode showed the best performance in the previous I_{sp} range, owing to its enhanced aerodynamic thrust.

References

[1]Jahn, R. G., *Physics of Electric Propulsion*, McGraw–Hill, New York, 1968.

[2]Toki, K., Shimizu, Y., and Kuriki, K., "Electric Propulsion Experiment (EPEX) of a Repetitively Pulsed MPD Thruster System Onboard Space Flyer Unit (SFU)," 25th International Electric Propulsion Conf., Paper 97-120, Aug. 1997.

[3]Myers, R. M., Mantenieks, M. A., and LaPointe, M. R., "MPD Thruster Technology," AIAA Paper 91-3568, Sept. 1991.

[4]Hack, K. J., George, J. A., Riehl, J. P., and Gilland, J. H., "Evolutionary Use of Nuclear Electric Propulsion," AIAA Paper 90-3821, Sept. 1990.

[5]Gilland, J. H., Myers, R. M., and Patterson, M. J., "Multimegawatt Electric Propulsion System Design Considerations," AIAA Paper 90-2552, July 1990.

[6]Jones, R. M., "Comparison of Potential Electric Propulsion Systems for Orbit Transfer," *Journal of Spacecraft and Rockets*, Vol. 21, No. 1, 1984, pp. 88–95.

[7]Frank, S. G., and Ronald, A. S., "Analysis of Hall-Effect Thrusters and Ion Engines for Orbit Transfer Missions," AIAA Paper 96-2973, July 1996.

[8]Auweter-Kurtz, M., Kurtz, H. L., and Schrade, H. O., "Optimization of Electric Propulsion Systems Considering Specific Power as Function of Specific Impulse," *Journal of Propulsion and Power*, Vol. 4, No. 6, 1988, pp. 512–519.

[9]Rudolph, L. K., "Design and Benefits of Pulsed MPD Thruster Orbit Transfer Vehicles," 17th International Electric Propulsion Conf., Paper 84-81, July 1984.

[10]Myers, R. M., Domonkos, M., and Gilland, J. H., "Low Power Pulsed MPD Thruster System Analysis and Applications," AIAA Paper 93-2391, June 1993.

[11]Domonkos, M., "Pulsed MPD Thruster Systems Analysis and Heated Cathodes," AIAA Paper 94-0007, Jan. 1994.

[12]Sovey, J. S., and Mantenieks, M. A., "Performance and Lifetime Assessment of Magnetoplasmadynamic Arc Thruster Technology," *Journal of Propulsion and Power*, Vol. 7, No. 1, 1991, pp. 71–83.

[13]Sumida, M., and Toki, K., "Scaling Law and Real Gas Effect of MPD Thruster," AIAA Paper 87-1066, May 1987.

[14]Kurtz, H. L., Auweter-Kurtz, M., Merke, W. D., and Schrade, H. O., "Experimental MPD Thruster Investigations," AIAA Paper 87-1019, May 1987.

[15]Wolff, M., Kelly, A. J., and Jahn, R. G., "A High Performance Magnetoplasmadynamic Thruster," 17th International Electric Propulsion Conf., Paper 84-32, July 1984.

[16]Uematsu, K., Mori, K., Kuninaka, H., and Kuriki, K., "Effect of Electrode Configuration on MPD Arcjet Performance," 17th International Electric Propulsion Conf., Paper 84-11, July 1984.

[17]Yoshikawa, T., Kagaya, Y., Yokoi, Y., and Tahara, H., "Performance Characteristics of Quasi-Steady MPD Thrusters," 17th International Electric Propulsion Conf., Paper 84-58, July 1984.

[18]Toki, K., Sumida, M., and Kuriki, K., "Multichannel Two-Dimensional Magnetoplasmadynamic Arcjet," *Journal of Propulsion and Power*, Vol. 8, No. 1, 1992, pp. 93–97.

[19]Nakayama, T., and Toki, K., and Kuriki, K., "Quantitative Imaging of the Magnetoplasmadynamic Flowfield," *Journal of Propulsion and Power*, Vol. 8, No. 6, 1992, pp. 1217–1223.

[20]Funaki, I., "Magnetohydrodynamic Flow in MPD Arcjet," Ph.D. Dissertation, Tokyo Univ., Tokyo, Japan, 1995 (in Japanese).

[21]King, D. Q., "Magnetogasdynamic Channel Flow for Design of Coaxial MPD Thrusters," Ph.D. Dissertation, Princeton Univ., Princeton, NJ, 1981.

[22]Sumida, M., and Toki, K., "Real-Gas Effect on the Magnetoplasmadynamic Arcjet," *Journal of Propulsion and Power*, Vol. 7, No. 6, 1991, pp. 1072–1074.